International Journal of Fracture **102:** 371–392, 2000.

Interaction among a row of ellipsoidal inclusions

NAO-AKI NODA, HITOSHI HAYASHIDA and KENJI TOMARI
Department of Mechanical Engineering, Kyushu Institute of Technology, Kitakyushu 804-8550, Japan, e-mail: noda@mech.kyutech.ac.jp

Received 14 January 1999; accepted in revised form 4 August 1999

Abstract. In this paper the interaction among a row of N ellipsoidal inclusions of revolution is considered. Inclusions in a body under both (A) asymmetric uniaxial tension in the x-direction and (B) axisymmetric uniaxial tension in the z-direction are treated in terms of singular integral equations resulting from the body force method. These problems are formulated as a system of singular integral equations with Cauchy-type or logarithmic-type singularities, where unknowns are densities of body forces distributed in the r, θ, z directions. In order to satisfy the boundary conditions along the ellipsoidal boundaries, the unknown functions are approximated by a linear combination of fundamental density functions and polynomials. The present method is found to yield rapidly converging numerical results for interface stresses. When the elastic ratio $E_1 \Rightarrow E_1/E_M > 1$, the primary feature of the interaction is a large compressive or tensile stress σ_n on the interface $\theta = 0$. When $E_1 \Rightarrow E_1/E_M < 1$, a large tensile stress σ_θ or σ_t on the interface $\theta = \frac{1}{2}\pi$ is of interest. If the spacing b/d and the elastic ratio E_1/E_M are fixed, the interaction effects are dominant when the shape ratio a/b is large. For any fixed shape and spacing of inclusions, the maximum stress is shown to be linear with the reciprocal of the squared number of inclusions.

Keywords: Elasticity, body force method, singular integral equations, numerical analysis, three-dimensional analysis, stress concentration factor, ellipsoidal inclusion.

1. Introduction

It is known that most engineering materials contain some defects in the form of cracks, voids, inclusions, or second-phased particles. To evaluate the effect of defects on the strength of structures, it is necessary to know the stress concentration of those defects. As a model of defects elliptical and ellipsoidal inclusions are important because they cover a wide variety of particular cases, such as line, circular, and spherical defects. In previous studies a single ellipsoidal inclusion (Atsumi, 1960; Edwards, 1952; Eshelby, 1957, 1959), 2 D elliptical inclusions (Donnel, 1941; Nisitani, 1968; Shioya, 1970; Isida–Igawa, 1994; Noda–Matsuo, 1997), and 3 D symmetric inclusion problems (Miyamoto, 1957; Nisitani, 1963; Eubank, 1965; Shelly–Yu, 1966; Goree–Wilson, 1967; Noda–Matsuo, 1995) are treated by several authors. However, few studies are made for 3 D asymmetric problems except for spherical cavities under asymmetric uniaxial tension treated by Tsuchida (1976, 1978) et al. and two ellipsoidal inclusions treated by Noda–Tomari–Matsuo (1999).

This paper deals with an interaction among a row of N ellipsoidal inclusions of revolution under (A) asymmetric and (B) axisymmetric uniaxial tension, which are formulated using the body force method coupled with a singular integral equation approach. Then, the interaction effects will be discussed by varying the shape, spacing and elastic ratio of the ellipsoidal inclusions.

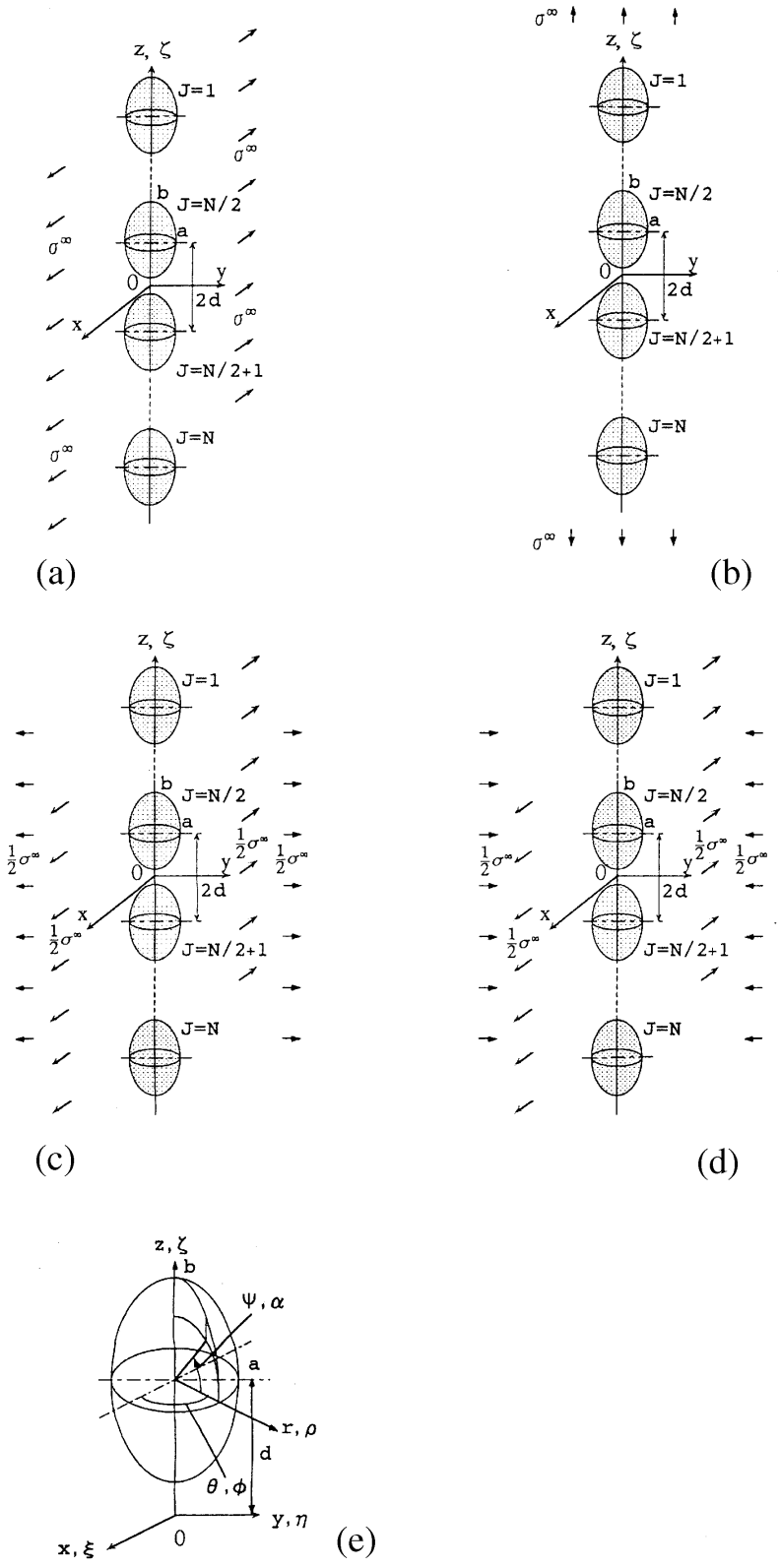

Figure 1. Problem and coordinate system; (a) Uniaxial tension perpendicular to the line of the inclusions (x-direction); (b) Uniaxial tension in the line of the inclusions (z-direction); (c) Hydrostatic tension in a plane perpendicular to the line of the inclusions (xy-plane); (d) Pure shear in a plane perpendicular to the line of the inclusions (xy-plane); (e) Coordinate system.

2. Method of analysis

Consider an infinite body having a row of N ellipsoidal inclusions in the z-direction. Method of analysis will be explained when uniaxial tension is applied asymmetrically in the x-direction as shown in Figure 1 (a). This problem is composed of the superposition of two auxiliary loads; biaxial tension in the xy-plane shown in Figure 1(c), and pure shear in the xy-plane shown in Figure 1(d). Rectangular and cylindrical coordinates (x, y, z) and (r, θ, z) are defined in Figure 1(e). Here, (ξ, η, ζ) and (ρ, ϕ, ζ) are rectangular and cylindrical coordinates that specify the points where body forces are distributed. In this paper, the solution of the problem of pure shear in the xy-plane will be mainly explained assuming the number of inclusions N is even. When N is odd, the problem can be solved in the same way except that at the innermost inclusion the boundary condition should be considered in the range $0 \leqslant \psi \leqslant \pi/2$.

The body force method (Nisitani, 1967) is used to formulate the problem as a system of singular integral equations. Here, the fundamental solutions are stress ($K_{nn}^{F_r}, K_{nn}^{F_\theta}, \ldots, K_{nt}^{F_\theta}, K_{nt}^{F_z}$) and displacement fields ($K_{ur}^{F_r}, K_{ur}^{F_\theta}, \ldots, K_{uz}^{F_\theta}, K_{uz}^{F_z}$) at an arbitrary point [$r = a \cos \psi_k, z = d + 2d(i-1) + b \sin \psi_k, i = 1 \sim N/2$] when two ring forces acting symetrically to the plane $z = 0$ [$\rho = a \cos \alpha_k, \zeta = \pm\{d + 2d(k-1) + b \sin \alpha_k\}, k = 1 \sim N/2$]. In this case the boundary conditions only on $z \geqslant 0$ can be considered due to symmetry. Since each ring force has a magnitude proportional to $\cos 2\varphi$ or $\sin 2\varphi$ along the circumference (Noguchi et al., 1987; Noda–Tomari, 1998), the problem can be formulated in terms of singular integral equations by using the fundamental solutions due to ring forces in two infinite bodies 'M' and 'I'. Here, the infinite body 'M' has the same elastic constants as those of the matrix (E_M, ν_M) and the infinite body 'I' has the same ones as those of the inclusions ($E_\mathrm{I}, \nu_\mathrm{I}$). The integral equations are expressed in terms of unknown body force densities $\rho_{rM}^*(\alpha_k)$, $\rho_{\theta M}^*(\alpha_k)$, $\rho_{zM}^*(\alpha_k)$ $\rho_{r\mathrm{I}}^*(\alpha_k)$, $\rho_{\theta\mathrm{I}}^*(\alpha_k)$, $\rho_{z\mathrm{I}}^*(\alpha_k)$ distributed at the infinitesimal area $\rho\, \mathrm{d}\phi\, \mathrm{d}s$ specified by the angle α_k. These equations are

$$
\begin{aligned}
&-\tfrac{1}{2}\{\rho_{rM}^*(\psi_i)\cos\psi_{i0} + \rho_{zM}^*(\psi_i)\sin\psi_{i0}\} \\
&-\tfrac{1}{2}\{\rho_{r\mathrm{I}}^*(\psi_i)\cos\psi_{i0} + \rho_{z\mathrm{I}}^*(\psi_i)\sin\psi_{i0}\} \\
&+\sum_{k=1}^{N/2}\int_{-\pi/2}^{\pi/2} K_{nnM}^{F_r}(\alpha_k, \psi_i)\rho_{rM}^*(\alpha_k)\,\mathrm{d}s + \sum_{k=1}^{N/2}\int_{-\pi/2}^{\pi/2} K_{nnM}^{F_\theta}(\alpha_k, \psi_i)\rho_{\theta M}^*(\alpha_k)\,\mathrm{d}s \\
&+\sum_{k=1}^{N/2}\int_{-\pi/2}^{\pi/2} K_{nnM}^{F_z}(\alpha_k, \psi_i)\rho_{zM}^*(\alpha_k)\,\mathrm{d}s - \sum_{k=1}^{N/2}\int_{-\pi/2}^{\pi/2} K_{nn\mathrm{I}}^{F_r}(\alpha_k, \psi_i)\rho_{r\mathrm{I}}^*(\alpha_k)\,\mathrm{d}s \\
&-\sum_{k=1}^{N/2}\int_{-\pi/2}^{\pi/2} K_{nn\mathrm{I}}^{F_\theta}(\alpha_k, \psi_i)\rho_{\theta\mathrm{I}}^*(\alpha_k)\,\mathrm{d}s - \sum_{k=1}^{N/2}\int_{-\pi/2}^{\pi/2} K_{nn\mathrm{I}}^{F_z}(\alpha_k, \psi_i)\rho_{z\mathrm{I}}^*(\alpha_k)\,\mathrm{d}s \\
&\quad = -\sigma_r^\infty \cos^2\psi_{i0}\cos 2\theta \qquad (1) \\
&-\tfrac{1}{2}\{\rho_{\theta M}^*(\psi_i) + \rho_{\theta\mathrm{I}}^*(\psi_i)\} \\
&+\sum_{k=1}^{N/2}\int_{-\pi/2}^{\pi/2} K_{n\theta M}^{F_r}(\alpha_k, \psi_i)\rho_{rM}^*(\alpha_k)\,\mathrm{d}s + \sum_{k=1}^{N/2}\int_{-\pi/2}^{\pi/2} K_{n\theta M}^{F_\theta}(\alpha_k, \psi_i)\rho_{\theta M}^*(\alpha_k)\,\mathrm{d}s
\end{aligned}
$$

$$+\sum_{k=1}^{N/2}\int_{-\pi/2}^{\pi/2} K_{n\theta M}^{F_z}(\alpha_k,\psi_i)\rho_{zM}^*(\alpha_k)\,\mathrm{d}s-\sum_{k=1}^{N/2}\int_{-\pi/2}^{\pi/2} K_{n\theta \mathrm{I}}^{F_r}(\alpha_k,\psi_i)\rho_{r\mathrm{I}}^*(\alpha_k)\,\mathrm{d}s$$

$$-\sum_{k=1}^{N/2}\int_{-\pi/2}^{\pi/2} K_{n\theta \mathrm{I}}^{F_\theta}(\alpha_k,\psi_i)\rho_{\theta\mathrm{I}}^*(\alpha_k)\,\mathrm{d}s-\sum_{k=1}^{N/2}\int_{-\pi/2}^{\pi/2} K_{n\theta \mathrm{I}}^{F_z}(\alpha_k,\psi_i)\rho_{z\mathrm{I}}^*(\alpha_k)\,\mathrm{d}s$$

$$=\tau_{r\theta}^{\infty}\ \sin\ \psi_{i0}\ \cos\ \psi_{i0}\ \sin\ 2\theta \tag{2}$$

$$-\tfrac{1}{2}\{-\rho_{rM}^*(\psi_i)\ \sin\ \psi_{i0}+\rho_{zM}^*(\psi_i)\ \cos\ \psi_{i0}\}$$

$$-\tfrac{1}{2}\{-\rho_{r\mathrm{I}}^*(\psi_i)\ \sin\ \psi_{i0}+\rho_{z\mathrm{I}}^*(\psi_i)\ \cos\ \psi_{i0}\}$$

$$+\sum_{k=1}^{N/2}\int_{-\pi/2}^{\pi/2} K_{ntM}^{F_r}(\alpha_k,\psi_i)\rho_{rM}^*(\alpha_k)\,\mathrm{d}s+\sum_{k=1}^{N/2}\int_{-\pi/2}^{\pi/2} K_{ntM}^{F_\theta}(\alpha_\kappa,\psi_i)\rho_{\theta M}^*(\alpha_\kappa)\,\mathrm{d}s$$

$$+\sum_{k=1}^{N/2}\int_{-\pi/2}^{\pi/2} K_{ntM}^{F_z}(\alpha_\kappa,\psi_i)\rho_{zM}^*(\alpha_\kappa)\,\mathrm{d}s-\sum_{k=1}^{N/2}\int_{-\pi/2}^{\pi/2} K_{nt\mathrm{I}}^{F_r}(\alpha_\kappa,\psi_i)\rho_{r\mathrm{I}}^*(\alpha_\kappa)\,\mathrm{d}s$$

$$-\sum_{k=1}^{N/2}\int_{-\pi/2}^{\pi/2} K_{nt\mathrm{I}}^{F_\theta}(\alpha_\kappa,\psi_i)\rho_{\theta\mathrm{I}}^*(\alpha_\kappa)\,\mathrm{d}s-\sum_{k=1}^{N/2}\int_{-\pi/2}^{\pi/2} K_{nt\mathrm{I}}^{F_z}(\alpha_\kappa,\psi_i)\rho_{z\mathrm{I}}^*(\alpha_\kappa)\,\mathrm{d}s$$

$$=\sigma_r^{\infty}\ \sin\ \psi_{i0}\ \cos\ \psi_{i0}\ \cos\ 2\theta \tag{3}$$

$$\sum_{k=1}^{N/2}\int_{-\pi/2}^{\pi/2} K_{urM}^{F_r}(\alpha_\kappa,\psi_i)\rho_{rM}^*(\alpha_\kappa)\,\mathrm{d}s+\sum_{k=1}^{N/2}\int_{-\pi/2}^{\pi/2} K_{urM}^{F_\theta}(\alpha_\kappa,\psi_i)\rho_{\theta M}^*(\alpha_\kappa)\,\mathrm{d}s$$

$$+\sum_{k=1}^{N/2}\int_{-\pi/2}^{\pi/2} K_{urM}^{F_z}(\alpha_\kappa,\psi_i)\rho_{zM}^*(\alpha_\kappa)\,\mathrm{d}s-\sum_{k=1}^{N/2}\int_{-\pi/2}^{\pi/2} K_{ur\mathrm{I}}^{F_r}(\alpha_\kappa,\psi_i)\rho_{r\mathrm{I}}^*(\alpha_\kappa)\,\mathrm{d}s$$

$$-\sum_{k=1}^{N/2}\int_{-\pi/2}^{\pi/2} K_{ur\mathrm{I}}^{F_\theta}(\alpha_\kappa,\psi_i)\rho_{\theta\mathrm{I}}^*(\alpha_\kappa)\,\mathrm{d}s-\sum_{k=1}^{N/2}\int_{-\pi/2}^{\pi/2} K_{ur\mathrm{I}}^{F_z}(\alpha_\kappa,\psi_i)\rho_{z\mathrm{I}}^*(\alpha_\kappa)\,\mathrm{d}s$$

$$=(\sigma_r^{\infty}-\nu_M\sigma_\theta^{\infty})r/E_M\ \cos\ 2\theta \tag{4}$$

$$\sum_{k=1}^{N/2}\int_{-\pi/2}^{\pi/2} K_{u\theta M}^{F_r}(\alpha_\kappa,\psi_i)\rho_{rM}^*(\alpha_\kappa)\,\mathrm{d}s+\sum_{k=1}^{N/2}\int_{-\pi/2}^{\pi/2} K_{u\theta M}^{F_\theta}(\alpha_\kappa,\psi_i)\rho_{\theta M}^*(\alpha_\kappa)\,\mathrm{d}s$$

$$+\sum_{k=1}^{N/2}\int_{-\pi/2}^{\pi/2} K_{u\theta M}^{F_z}(\alpha_\kappa,\psi_i)\rho_{zM}^*(\alpha_\kappa)\,\mathrm{d}s-\sum_{k=1}^{N/2}\int_{-\pi/2}^{\pi/2} K_{u\theta\mathrm{I}}^{F_r}(\alpha_\kappa,\psi_i)\rho_{r\mathrm{I}}^*(\alpha_\kappa)\,\mathrm{d}s$$

$$-\sum_{k=1}^{N/2}\int_{-\pi/2}^{\pi/2} K_{u\theta\mathrm{I}}^{F_\theta}(\alpha_\kappa,\psi_i)\rho_{\theta\mathrm{I}}^*(\alpha_\kappa)\,\mathrm{d}s-\sum_{k=1}^{N/2}\int_{-\pi/2}^{\pi/2} K_{u\theta\mathrm{I}}^{F_z}(\alpha_\kappa,\psi_i)\rho_{z\mathrm{I}}^*(\alpha_\kappa)\,\mathrm{d}s$$

$$=-\tau_{r\theta}^{\infty}2(1+\nu_M)r/E_M\cdot\sin\ 2\theta \tag{5}$$

$$\sum_{k=1}^{N/2}\int_{-\pi/2}^{\pi/2} K_{uzM}^{F_r}(\alpha_\kappa, \psi_i)\rho_{rM}(\alpha_\kappa)\,\mathrm{d}s + \sum_{k=1}^{N/2}\int_{-\pi/2}^{\pi/2} K_{uzM}^{F_\theta}(\alpha_\kappa, \psi_i)\rho_{\theta M}^*(\alpha_\kappa)\,\mathrm{d}s$$
$$+ \sum_{k=1}^{N/2}\int_{-\pi/2}^{\pi/2} K_{uzM}^{F_z}(\alpha_\kappa, \psi_i)\rho_{zM}^*(\alpha_\kappa)\,\mathrm{d}s - \sum_{k=1}^{N/2}\int_{-\pi/2}^{\pi/2} K_{uz\mathrm{I}}^{F_r}(\alpha_\kappa, \psi_i)\rho_{r\mathrm{I}}^*(\alpha_\kappa)\,\mathrm{d}s$$
$$- \sum_{k=1}^{N/2}\int_{-\pi/2}^{\pi/2} K_{uz\mathrm{I}}^{F_\theta}(\alpha_\kappa, \psi_i)\rho_{\theta\mathrm{I}}^*(\alpha_\kappa)\,\mathrm{d}s - \sum_{k=1}^{N/2}\int_{-\pi/2}^{\pi/2} K_{uz\mathrm{I}}^{F_z}(\alpha_\kappa, \psi_i)\rho_{z\mathrm{I}}^*(\alpha_\kappa)\,\mathrm{d}s$$
$$= -\nu_M(\sigma_r^\infty + \sigma_\theta^\infty)z/E_M\ \cos\ 2\theta \tag{6}$$

$i = 1 \sim \frac{1}{2}N$

where

$$-\mathrm{d}\rho = a\ \sin\ \alpha_k\,\mathrm{d}\alpha_k,\ \mathrm{d}\zeta = b\ \cos\ \alpha_k\,\mathrm{d}\alpha_k, \qquad \mathrm{d}s = \sqrt{a^2\ \sin^2\ \alpha_k + b^2\ \cos^2\ \alpha_k}\,\mathrm{d}\alpha_k$$

Here ψ_0 is the angle between the r-axis and the normal direction of the ellipsoidal inclusion at (r, z), and the cos 2θ and sin 2θ terms in (1)–(6) express a plane state of shear at $r \to \infty$. The notation $\sum_{k=1}^{N/2}$ means integrating the effect of body force density along the prospective boundary for inclusions. The unknown functions in (1)–(6) $\rho_{rM}^*(\alpha_k)$, $\rho_{\theta M}^*(\alpha_k)$, $\rho_{zM}^*(\alpha_k)$ are defined by the following equations. Other unknown functions $\rho_{r\mathrm{I}}^*(\alpha_k)$, $\rho_{\theta\mathrm{I}}^*(\alpha_k)$, $\rho_{z\mathrm{I}}^*(\alpha_k)$ can be expressed in a similar way.

$$\rho_{rM}^*(\alpha_k)\ \cos\ 2\varphi = \frac{\mathrm{d}F_r}{\rho\,\mathrm{d}\phi\,\mathrm{d}s}, \qquad \rho_{\theta M}^*(\alpha_k)\ \sin\ 2\varphi = \frac{\mathrm{d}F_\theta}{\rho\,\mathrm{d}s\,\mathrm{d}\phi},$$
$$\rho_{zM}^*(\alpha_k)\ \cos\ 2\varphi = \frac{-\mathrm{d}F_z}{\rho\,\mathrm{d}\phi\,\mathrm{d}s}. \tag{7}$$

Here $\mathrm{d}F_r$, $\mathrm{d}F_\theta$, $\mathrm{d}F_z$ are the components of the resultant of the body force in the r, θ, z directions, respectively, acting on the infinitesimal area $\rho\,\mathrm{d}\phi\,\mathrm{d}s$. Equations (1)–(6) enforce boundary conditions at the imaginary boundary; that is, $\sigma_{nM} - \sigma_{n\mathrm{I}} = 0$, $\tau_{ntM} - \tau_{nt\mathrm{I}} = 0$, $\tau_{n\theta M} - \tau_{n\theta\mathrm{I}} = 0$, $u_{rM} - u_{r\mathrm{I}} = 0$, $u_{zM} - u_{z\mathrm{I}} = 0$, $u_{\theta M} - u_{\theta\mathrm{I}} = 0$. It should be noted that (1)–(3) include the Cauchy-type singularities and (4)–(6) include the logarithmic-type singularities. Therefore in (1)–(3), the integration should be interpreted in the Cauchy principal value sense.

As shown in (1)–(6), the problem is reduced to determining the body force densities $\rho_{rM}^*(\alpha_k) \sim \rho_{z\mathrm{I}}^*(\alpha_k)$. In the present method, however, auxiliary functions ($f_1(\alpha)$, $f_2(\alpha)$), which are defined in terms of original unknowns, will be determined. In the following equations, the notation $f(\alpha)$ refers to the original unknowns $\rho_{rM}^*(\alpha_k) \sim \rho_{z\mathrm{I}}^*(\alpha_k)$, and $f_1(\alpha_k)$, $f_2(\alpha_k)$ refers to the auxiliary functions defined by (Noda–Matsuo, 1998)

$$f_1(\alpha_k) = \{f(\alpha_k) + f(-\alpha_k)\}/2,\ f_2(\alpha_k) = \{f(\alpha_k) - f(-\alpha_k)\}/2, \tag{8}$$

where

$$f_1(\alpha_k) = f_1(-\alpha_k),\ f_2(\alpha_k) = -f_2(-\alpha_k). \tag{9}$$

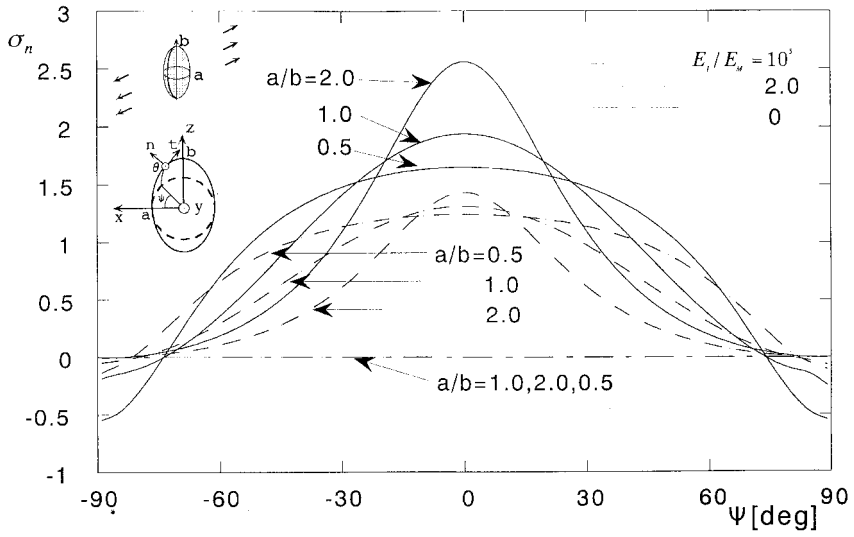

Figure 2. Interface stress σ_n on $\theta = 0$ for a single inclusion for uniaxial tension in the x-direction ($N = 1$, $a/b = 0.5, 1.0, 2.0$, $E_1/E_M = 10^5, 2.0, 0$).

These relations show that determining the auxiliary functions $f_1(\alpha_k)$, $f_2(\alpha_k)$ in the range $0 \leqslant \alpha_k \leqslant \frac{1}{2}/\pi$ is equivalent to determining the unknown functions $f(\alpha_k)$ in the range $-\frac{1}{2}\pi \leqslant \alpha_k \leqslant \frac{1}{2}\pi$. In other words, if the auxiliary functions are given in the range $0 \leqslant \alpha_k \leqslant \frac{1}{2}\pi$, the original unknown functions $f(\alpha_k)$ are expressed in the range $-\frac{1}{2}\pi \leqslant \alpha_k \leqslant \frac{1}{2}\pi$ as follows.

$$\begin{aligned} &f(\alpha_k) = f_1(\alpha_k) + f_2(\alpha_k), \\ &f(-\alpha_k) = f_1(-\alpha_k) + f_2(-\alpha_k) = f_1(\alpha_k) - f_2(\alpha_k). \end{aligned} \tag{10}$$

Then, fundamental density functions are defined by (11) as examples of continuous functions satisfying (10). Here, it should be noted that $w_{r3}(\alpha_k)$, $w_{\theta 3}(\alpha_k)$, $w_{z2}(\alpha_k)$ are exact densities of body force to express a single ellipsoidal inclusion under plane state of pure shear.

$$\begin{aligned} &w_{r3}(\alpha_k) = w_{\theta 3}(\alpha_k) = n_r(\alpha_k),\ w_{r4}(\alpha_k) = w_{\theta 4}(\alpha_k) = n_r(\alpha_k) \sin \alpha_k, \\ &w_{z1}(\alpha_k) = n_z(\alpha_k)/\sin \alpha_k,\ w_{z2}(\alpha_k) = n_z(\alpha_k). \end{aligned} \tag{11}$$

$$n_r(\alpha_k) = \frac{b \cos \alpha_k}{\sqrt{a^2 \sin^2 \alpha_k + b^2 \cos^2 \alpha_k}},\ n_z(\alpha_k) = \frac{a \sin \alpha_k}{\sqrt{a^2 \sin^2 \alpha_k + b^2 \cos^2 \alpha_k}}. \tag{12}$$

In (11), $w_{r3}(\alpha_k)$, $w_{\theta 3}(\alpha_k)$, $w_{z2}(\alpha_k)$ satisfy the first (9), and $w_{r4}(\alpha_k)$, $w_{\theta 4}(\alpha_k)$, $w_{z1}(\alpha_k)$ satisfy the second (9). The unknown functions $\rho^*_{rM}(\alpha_k) \sim \rho^*_{z\mathrm{I}}(\alpha_k)$ can be expressed as a linear com-

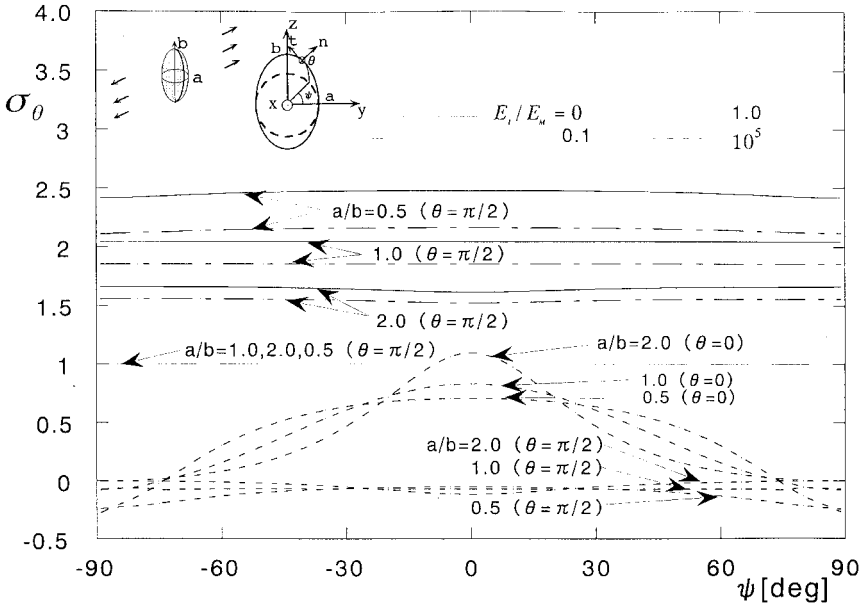

Figure 3. Interface stress σ_θ on $\theta = \frac{1}{2}\pi$ for a single inclusion for uniaxial tension in the x-direction ($N = 1$, $a/b = 0.5, 1.0, 2.0$, $E_I/E_M = 10^5, 1.0, 0.1, 0$).

bination of the fundamental density functions and weight functions as shown in the following equations.

$$\begin{aligned}
\rho^*_{rM}(\alpha_k) &= \rho_{r3M}(\alpha_k)w_{r3}(\alpha_k) + \rho_{r4M}(\alpha_k)w_{r4}(\alpha_k),\\
\rho^*_{\theta M}(\alpha_k) &= \rho_{\theta 3M}(\alpha_k)w_{\theta 3}(\alpha_k) + \rho_{\theta 4M}(\alpha_k)w_{\theta 4}(\alpha_k),\\
\rho^*_{zM}(\alpha_k) &= \rho_{z2M}(\alpha_k)w_{z2}(\alpha_k) + \rho_{z1M}(\alpha_k)w_{z1}(\alpha_k),\\
\rho^*_{r\mathrm{I}}(\alpha_k) &= \rho_{r3\mathrm{I}}(\alpha_k)w_{r3}(\alpha_k) + \rho_{r4\mathrm{I}}(\alpha_k)w_{r4}(\alpha_k),\\
\rho^*_{\theta\mathrm{I}}(\alpha_k) &= \rho_{\theta 3\mathrm{I}}(\alpha_k)w_{\theta 3}(\alpha_k) + \rho_{\theta 4\mathrm{I}}(\alpha_k)w_{\theta 4}(\alpha_k),\\
\rho^*_{z\mathrm{I}}(\alpha_k) &= \rho_{z2\mathrm{I}}(\alpha_k)w_{z2}(\alpha_k) + \rho_{z1\mathrm{I}}(\alpha_k)w_{z1}(\alpha_k).
\end{aligned} \tag{13}$$

In (13), taking $\rho^*_{rM}(\alpha_k)$ for example, $\rho_{r3M}(\alpha_k)w_{r3}(\alpha_k)$ corresponds to $f_1(\alpha_k)$ of (10) and $\rho_{r4M}(\alpha_k)w_{r4}(\alpha_k)$ corresponds to $f_2(\alpha_k)$ of (10). Then, all weight functions $\rho^*_{rM}(\alpha_k) \sim \rho^*_{z\mathrm{I}}(\alpha_k)$ must satisfy

$$g(\alpha_k) = g(-\alpha_k), \tag{14}$$

where $g(\alpha_k)$ refers to the weight functions $\rho_{r3M}(\alpha_k), \rho_{r4M}(\alpha_k), \ldots, \rho_{z1\mathrm{I}}(\alpha_k)$. In this study, the following equations have been applied.

Table 1. Convergence of the stress is for biaxial tension in the xy-plane, pure shear in the xy-plane, and uniaxial tension in the x-direction ($a/b = 1.0$, $b/d = 0.8$, $N = 3$, $J = 2$, $E_1/E_M = 10^5$, $\theta = 0$).

ψ (deg.)	M	Biaxal	Pure shear	Uniaxial
	16	1.7464	1.9910	3.7374
	20	1.7443	1.9913	3.7356
0.0	24	1.7442	1.9914	3.7356
	28	1.7441	1.9907	3.7348
	32	1.7440	1.9904	3.7344
	16	1.6819	1.9298	3.6117
	20	1.6801	1.9301	3.6102
10.0	24	1.6800	1.9299	3.6099
	28	1.6800	1.9297	3.6097
	32	1.6800	1.9292	3.6092
	16	1.1899	1.4909	2.6808
	20	1.1915	1.4909	2.6824
30.0	24	1.1915	1.4908	2.6823
	28	1.1916	1.4908	2.6824
	32	1.1915	1.4909	2.6824
	16	−0.3889	0.5337	0.1448
	20	−0.3681	0.5337	0.1656
60.0	24	−0.3672	0.5337	0.1665
	28	−0.3670	0.5337	0.1667
	32	−0.3669	0.5337	0.1668
	16	−2.1958	0.0002	−2.1956
	20	−2.1475	0.0002	−2.1473
90.0	24	−2.1455	0.0002	−2.1453
	28	−2.1450	0.0002	−2.1448
	32	−2.1449	0.0002	−2.1447

$$
\begin{aligned}
\rho_{r3M}(\alpha_k) &= \sum_{n=1}^{M/2} a_{knM} t_n(\alpha_k),\ \rho_{r3\mathrm{I}}(\alpha_k) = \sum_{n=1}^{M/2} a_{kn\mathrm{I}} t_n(\alpha_k),\\
\rho_{r4M}(\alpha_k) &= \sum_{n=1}^{M/2} b_{knM} t_n(\alpha_k),\ \rho_{r4\mathrm{I}}(\alpha_k) = \sum_{n=1}^{M/2} b_{kn\mathrm{I}} t_n(\alpha_k),\\
\rho_{r3M}(\alpha_k) &= \sum_{n=1}^{M/2} c_{knM} t_n(\alpha_k),\ \rho_{\theta 3\mathrm{I}}(\alpha_k) = \sum_{n=1}^{M/2} c_{kn\mathrm{I}} t_n(\alpha_k),\\
\rho_{r4M}(\alpha_k) &= \sum_{n=1}^{M/2} d_{knM} t_n(\alpha_k),\ \rho_{\theta 4\mathrm{I}}(\alpha_k) = \sum_{n=1}^{M/2} d_{kn\mathrm{I}} t_n(\alpha_k),\\
\rho_{z2M}(\alpha_k) &= \sum_{n=1}^{M/2} e_{knM} t_n(\alpha_k),\ \rho_{z2\mathrm{I}}(\alpha_k) = \sum_{n=1}^{M/2} e_{kn\mathrm{I}} t_n(\alpha_k),\\
\rho_{z1M}(\alpha_k) &= \sum_{n=1}^{M/2} f_{knM} t_n(\alpha_k),\ \rho_{z1\mathrm{I}}(\alpha_k) = \sum_{n=1}^{M/2} f_{kn\mathrm{I}} t_n(\alpha_k).
\end{aligned}
\tag{15}
$$

Table 2. Maximum stress of three spherical cavities for uniaxial tension in the x-direction ($N = 3$, $a/b = 1.0$, $E_{\mathrm{I}}/E_M = 0$).

a/d	$J = 1$				$J = 2$		
	ψ (deg.)	$K_{t\max}$	K_{ta}	K_{tb}	ψ (deg.)	$K_{t\max}$	K_{tc}
0	−90∼90	2.0454	2.0454	2.0454	−90∼90	2.0454	2.0454
	(−90∼90)	(2.045)	(2.045)	(2.045)	(−90∼90)	(2.045)	(2.045)
0.1	−7	2.0455	2.0452	2.0451	0	2.0456	2.0454
0.2	−7	2.0463	2.0455	2.0446	±1	2.0469	2.0447
	(−10)	(2.046)	(2.045)	(2.045)	(0)	(2.047)	(2.045)
0.3	−13	2.0484	2.0455	2.0424	±1	2.0503	2.0427
0.4	−17	2.0528	2.0464	2.0372	±2	2.0571	2.0385
	(−15)	(2.053)	(2.046)	(2.038)	(0)	(2.057)	(2.039)
0.5	−23	2.0613	2.0483	2.0300	±3	2.0687	2.0329
0.6	−30	2.0769	2.0519	2.0295	±17	2.0869	2.0347
	(−30)	(2.077)	(2.052)	(2.031)	(±15)	(2.087)	(2.036)
0.7	−41	2.1066	2.0573	2.0690	±36	2.1186	2.0767
0.8	−90	2.2449	2.0650	2.2449	±90	2.2540	2.2540
	(−90)	(2.241)	(2.265)	(2.241)	(±90)	(2.251)	(2.251)
0.9	−90	2.8263	2.0757	2.8263	±90	2.8345	2.8345

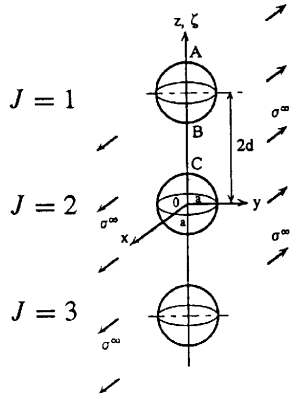

$$t_n(\alpha_k) = \cos\{2(n-1)\alpha_k\}. \tag{16}$$

The expressions (15) with (16) satisfy (14). Here M is number of collocation points in the range $-\frac{1}{2}\pi \leqslant \alpha_k \leqslant \frac{1}{2}\pi$. Then, the singular integral equations are reduced to a system of algebraic equations for determining the coefficients a_{nM}, b_{nM}, c_{nM}, d_{nM}, e_{nM}, f_{nM}, $a_{n\mathrm{I}}$, $b_{n\mathrm{I}}$, $c_{n\mathrm{I}}$, $d_{n\mathrm{I}}$, $e_{n\mathrm{I}}$, $f_{n\mathrm{I}}$. The number of unknown coefficients is $6M \times \frac{1}{2}N$. Using the numerical solution mentioned above the stress distribution along the interface can be determined. In the next section results for the maximum stresses are presented for various geometries and loading conditions.

3. Results and discussion

3.1. THE SINGLE INCLUSION

In Figure 2, an interface stress σ_n on $\theta = 0$ is plotted as a function on ψ when a single ellipsoidal inclusion is under uniaxial tension in the x-direction. In Figure 3, an interface stress σ_θ on $\theta = \frac{1}{2}\pi$ is plotted under the same condition. When the elastic ratio $E_I/E_M = 10^5$, σ_θ on $\theta = 0$ is also shown in Figure 3 because the value is larger than the one on $\theta = \frac{1}{2}\pi$. For a single inclusion we can see the maximum stresses for different values of E_I/E_M. When $E_I/E_M > 1$, the normal interface stresses σ_n are important because they may cause debonding of the interface. On the other hand, when $E_I/E_M < 1$, tangential interface stresses σ_θ are important because they are larger than other stresses. In the following section Poisson's ratios are set as $\nu_M = \nu_I = 0.3$.

3.2. CONVERGENCE OF THE RESULTS

Table 1 shows the convergence of the interface stress σ_n on $\theta = 0$ for biaxial tension in the xy-plane, pure shear in the xy-plane, and uniaxial tension in the x-direction in Figure 1 with increasing values of the collocation number M for $a/b = 1.0$, $b/d = 0.8$, $E_I/E_M = 10^5$. The present results have shown good convergence to the fourth digit when $M = 24$. Also the boundary conditions are confirmed to be less than 10^{-4} for $\sigma_{nM} - \sigma_{nI}$, $\tau_{n\theta M} - \tau_{n\theta I}$, $\tau_{ntM} - \tau_{ntI}$, $u_{rM} - u_{rI}$, $u_{\theta M} - u_{\theta I}$, $u_{zM} - u_{zI}$. This shows that the present method yields rapidly converging results and highly satisfied boundary conditions.

3.3. A ROW OF SEVERAL ELLIPSOIDAL INCLUSIONS

Results of cavities ($E_I/E_M = 0$) will be shown. Table 2 indicates the maximum stresses as function of position and the stresses at points A, B and C are indicated for three spherical cavities ($a/b = 1.0$). Here, points A, B, and C are indicated in the figure of Table 2. Tuchida's results (1978) coincide with the present results to the fourth digit in most cases.

Interface stresses σ_θ at the inclusions $J = 1 \sim 3$ are compared in Figure 4 when $N = 5$, $b/d = 0.9$, $a/b = 1.0$ for uniaxial tension in the x-direction. The stresses at $J = 2$ and $J = 3$ are almost equal although the stress at $J = 1$ is different. If N is fixed, it is not known which inclusion has the maximum stress as this depends on the values of E_I/E_M, b/d, and a/b. In the following section, the interaction will be discussed by choosing the innermost inclusion for uniaxial tension in the x- and z-direction.

Figures 5–10 shows the interface stress at the innermost inclusion when $N = 1 \sim 5$ for uniaxial tension in the x-direction. When $E_I/E_M > 1$, the primary feature of the interaction is a large compressive stress σ_n around $\psi = \pm\frac{1}{2}\pi$. However, the maximum tensile stress σ_n near $\psi = 0$, which may cause debonding of the interface, is almost independent of the interaction. When $E_I/E_M < 1$, a large tensile stress σ_θ on $\theta = \frac{1}{2}\pi$ is of interest. When b/d and E_I/E_M are fixed, the interaction appears largely when a/b is large for both cases $E_I/E_M > 1$ and $E_I/E_M < 1$.

Figures 11, 12 shows the interface stress at the innermost inclusion when $N = 1 \sim 5$ for uniaxial tension in the z-direction. When $E_I/E_M > 1$, the primary feature of the interaction is a large tensile stress σ_n at $\psi = \pm\frac{1}{2}\pi$. When $E_I/E_M < 1$, a large tensile stress σ_t around $\psi = 0$ is of interest. Generally, the interaction for uniaxial tension in the z-direction is larger than the one for uniaxial tension in the x-direction.

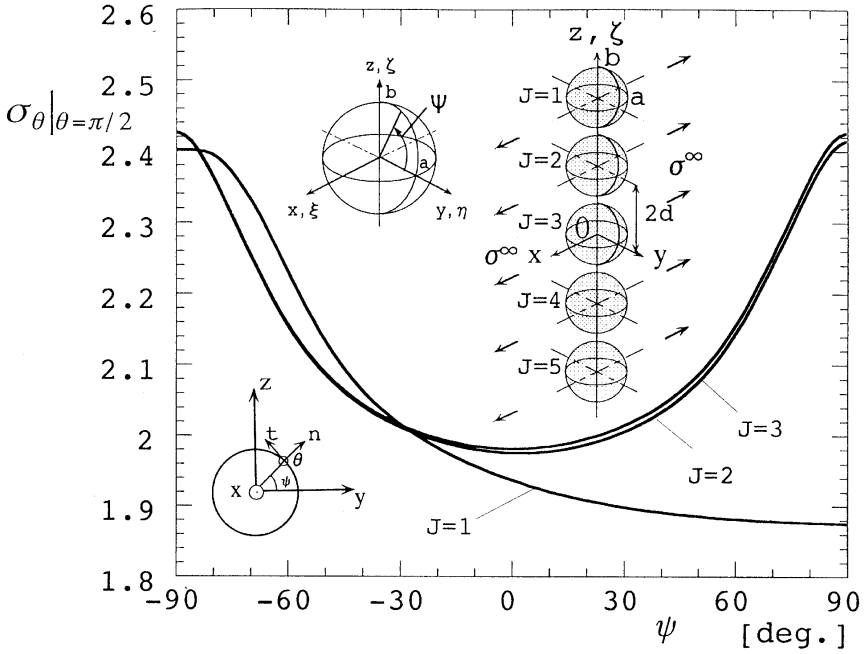

Figure 4. Interface stress σ_θ on $\theta = \frac{1}{2}\pi$ for uniaxial tension in the x-direction ($N = 5$, $a/b = 1.0$, $b/d = 0.9$, $E_1/E_M = 0.1$).

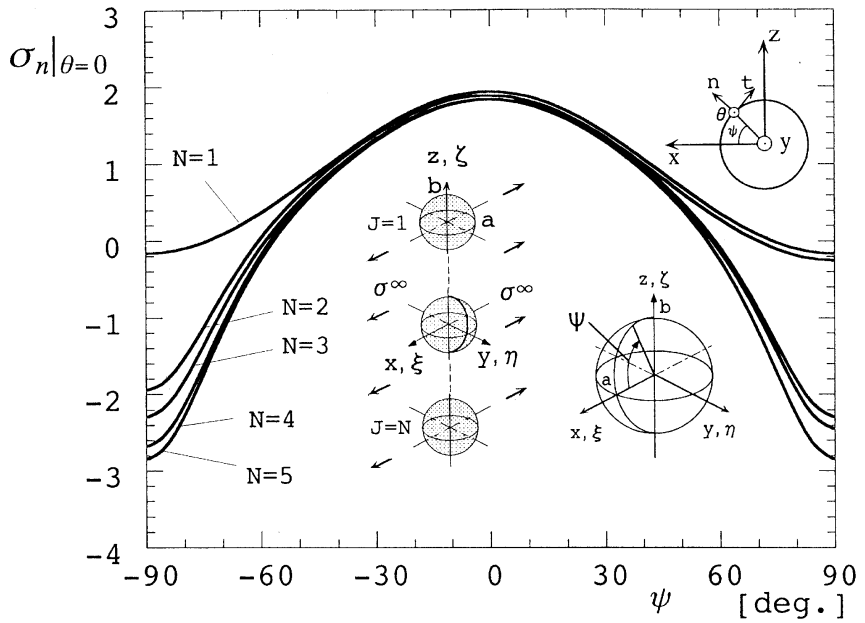

Figure 5. Interface stress σ_n on $\theta = 0$ for uniaxial tension in the x-direction ($N = 1 \sim 5$, $a/b = 1.0$, $b/d = 0.9$, $E_1/E_M = 10^5$).

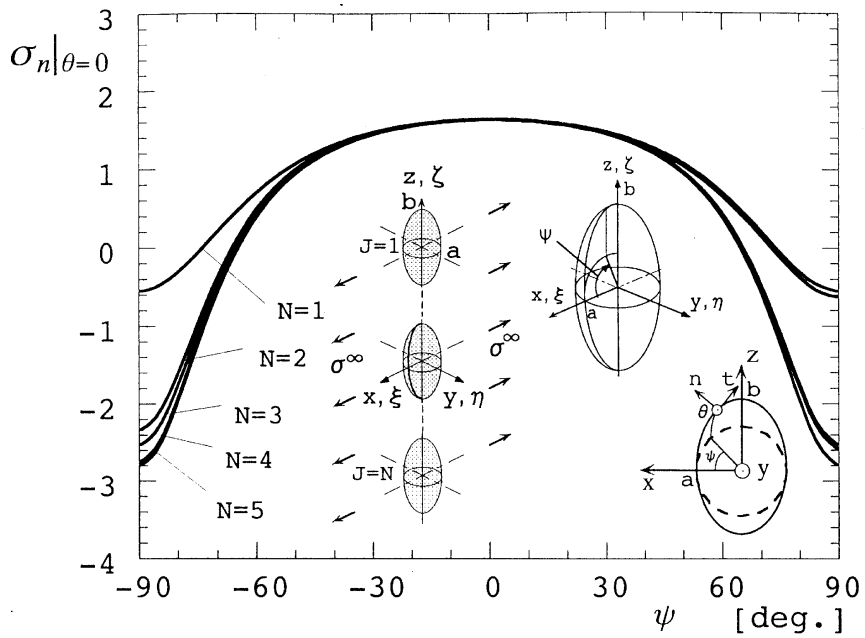

Figure 6. Interface stress σ_n on $\theta = 0$ for uniaxial tension in the x-direction ($N = 1 \sim 5$, $a/b = 0.5$, $b/d = 0.9$, $E_1/E_M = 10^5$).

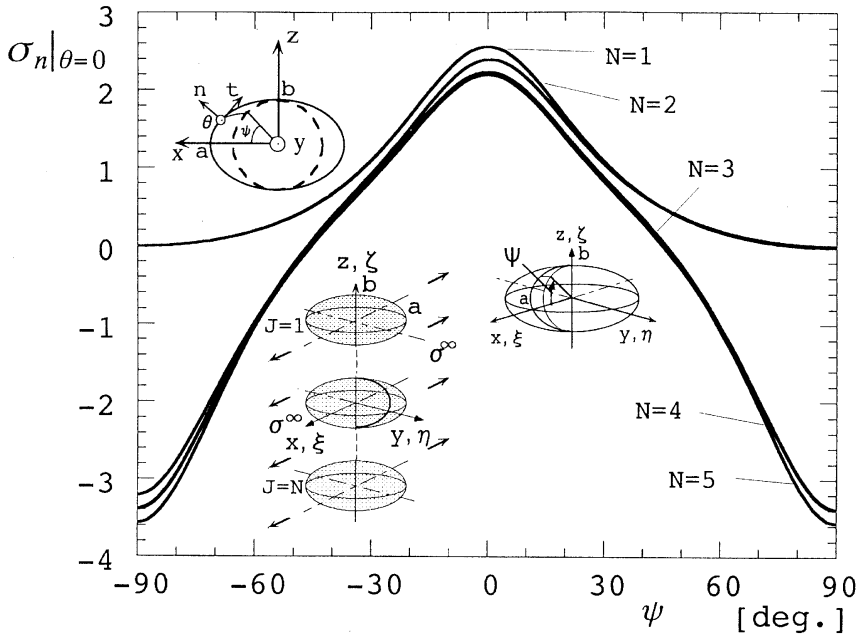

Figure 7. Interface stress σ_n on $\theta = 0$ for uniaxial tension in the x-direction ($N = 1 \sim 5$, $a/b = 2.0$, $b/d = 0.9$, $E_1/E_M = 10^5$).

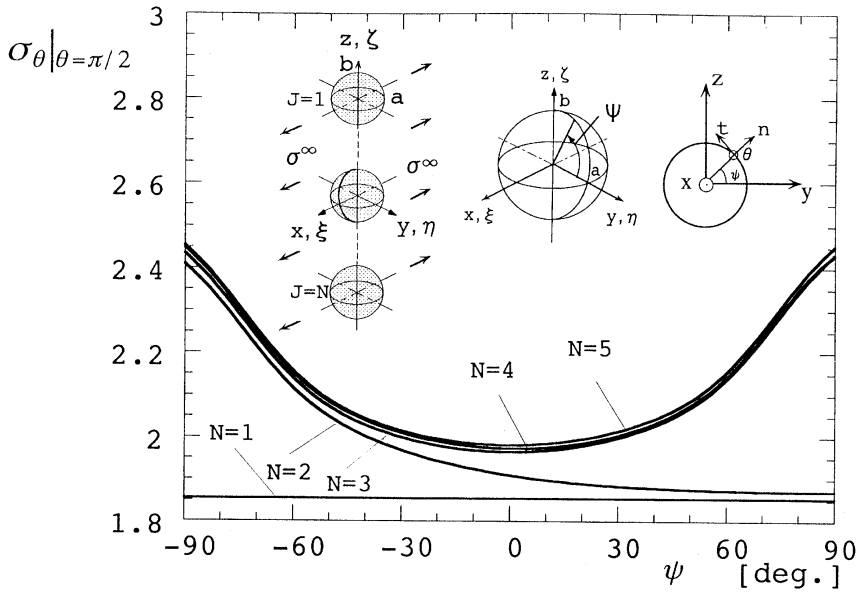

Figure 8. Interface stress σ_θ on $\theta = \frac{1}{2}\pi$ for uniaxial tension in the x-direction ($N = 1 \sim 5, a/b = 1.0, b/d = 0.9$, $E_1/E_M = 0.1$).

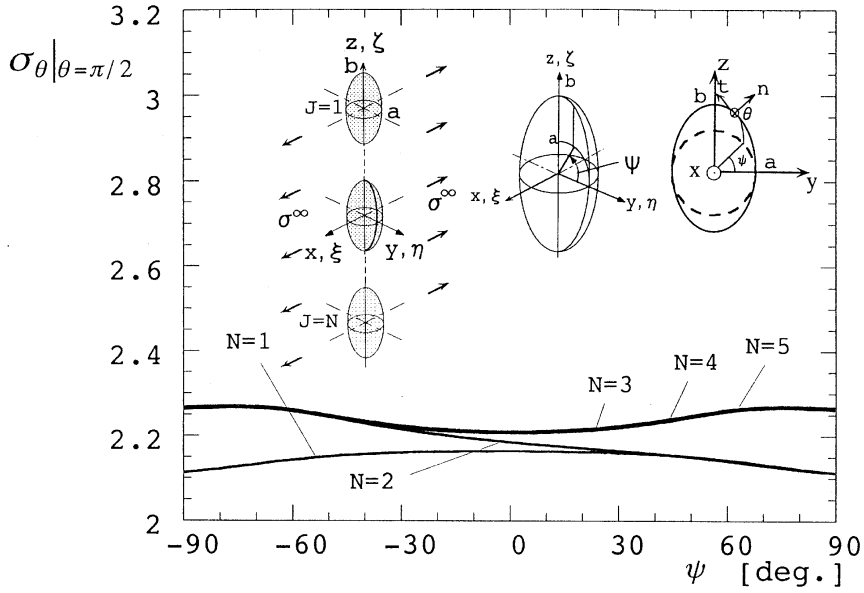

Figure 9. Interface stress σ_θ on $\theta = \frac{1}{2}\pi$ for uniaxial tension in the x-direction ($N = 1 \sim 5, a/b = 0.5, b/d = 0.9$, $E_1/E_M = 0.1$).

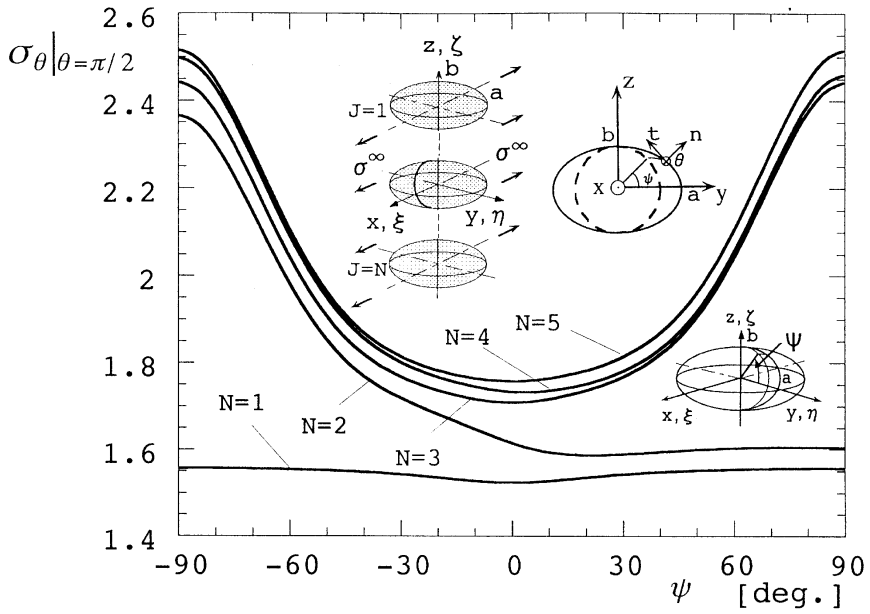

Figure 10. Interface stress σ_θ on $\theta = \frac{1}{2}\pi$ for uniaxial tension in the x-direction ($N = 1 \sim 5$, $a/b = 2.0$, $b/d = 0.9$, $E_1/E_M = 0.1$).

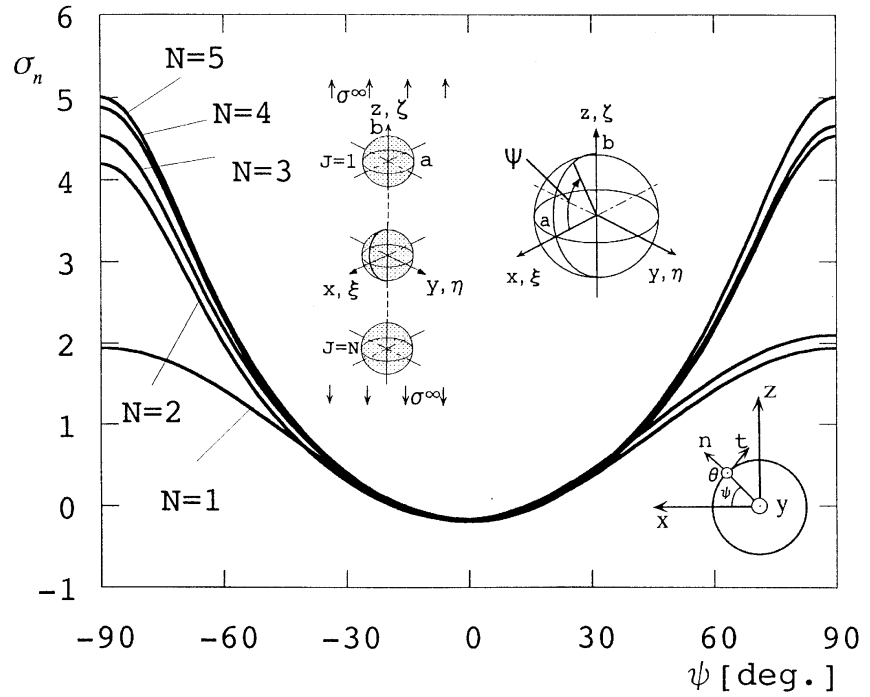

Figure 11. Interface stress σ_n for uniaxial tension in the z-direction ($N = 1 \sim 5$, $a/b = 1.0$, $b/d = 0.8$, $E_1/E_M = 10^5$).

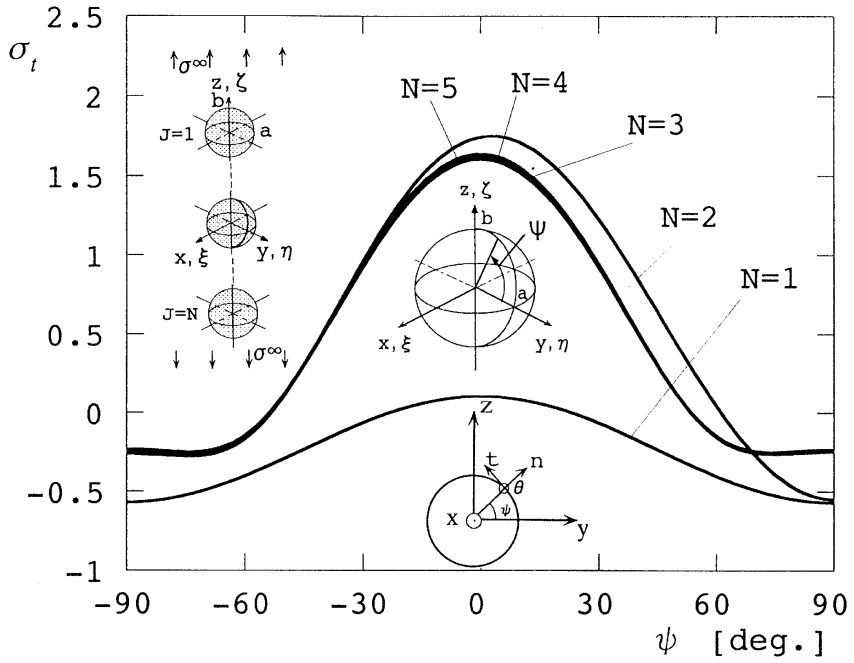

Figure 12. Interface stress σ_t for uniaxial tension in the z-direction ($N = 1 \sim 5$, $a/b = 1.0$, $b/d = 0.8$, $E_1/E_M = 0.1$).

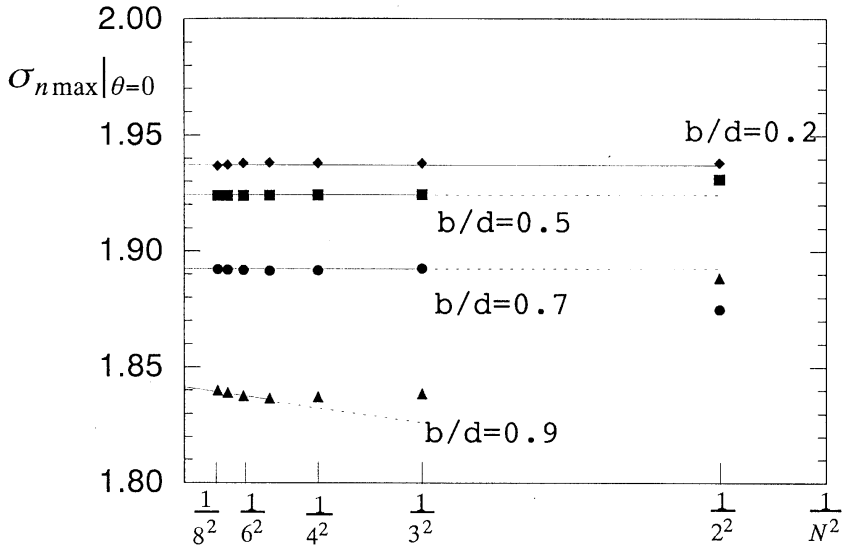

Figure 13. Maximum stress vs. $1/N^2$ relation for uniaxial tension in the x-direction ($a/b = 1.0$, $E_1/E_M = 10^5$, $\theta = 0$).

Table 3. Maximum stress of ellipsoidal inclusions for uniaxial tension in the x-direction ($N \to \infty$, $a/b = 1.0$).

$a/b = 1.0$		Matrix			
E_I/E_M	b/d	ψ (deg.)	σ_n	ψ (deg.)	σ_θ
					$\theta = \frac{1}{2}\pi$
	0			−90∼90	2.046
	0.2			±1	2.047
	0.5			±6	2.033
0.0	0.7			±34	2.131
	0.8			±90	2.279
	0.9			±90	2.888
			$\theta = 0$		$\theta = \frac{1}{2}\pi$
	0	0	0.192	0	1.854
	0.2	0	0.192	±3	1.855
	0.5	0	0.195	±3	1.879
0.1	0.7	0	0.199	±35	1.915
	0.8	0	0.204	±90	2.023
	0.9	0	0.209	±90	2.454
			$\theta = 0$		$\theta = 0$
	0	0	1.768	0	0.670
	0.2	0	1.768	0	0.670
	0.5	0	1.756	0	0.667
10	0.7	0	1.728	0	0.658
	0.8	0	1.705	0	0.651
	0.9	0	1.677	0	0.643
			$\theta = 0$		$\theta = 0$
	0	0	1.938	0	0.831
	0.2	0	1.936	0	0.834
	0.5	0	1.924	0	0.825
10^5	0.7	0	1.892	0	0.811
	0.8	0	1.869	0	0.800
		±90	(−1.393)	±90	(−0.592)
	0.9	0	1.843	0	0.790
		±90	(−3.101)	±90	(−1.351)

Table 4. Maximum stress of ellipsoidal inclusions for uniaxial tension in the x-direction ($N \to \infty$, $a/b = 2.0$).

$a/b = 2.0$		Matrix			
E_I/E_M	b/d	ψ (deg.)	σ_n	ψ (deg.)	σ_θ
					$\theta = \frac{1}{2}\pi$
	0			0	1.660
	0.2			±90	1.655
	0.5			±14	1.696
0	0.7			±90	1.970
	0.8			±90	2.332
	0.9			±90	3.112
			$\theta = 0$		$\theta = \frac{1}{2}\pi$
	0	0	0.156	0	1.524
	0.2	±1	0.157	±90	1.554
	0.5	±1	0.165	±26	1.583
0.1	0.7	±1	0.173	±90	1.794
	0.8	±1	0.176	±90	2.057
	0.9	±1	0.176	±90	2.554
			$\theta = 0$		$\theta = 0$
	0	0	2.208	0	0.834
	0.2	0	2.207	0	0.834
	0.5	0	2.130	0	0.808
10	0.7	0	2.033	0	0.761
	0.8	0	1.986	0	0.756
	0.9	0	1.934	0	0.742
			$\theta = 0$		$\theta = 0$
	0	0	2.557	0	1.096
	0.2	0	2.556	0	1.095
	0.5	0	2.448	0	1.049
10^5	0.7	0	2.313	0	0.990
	0.8	0	2.246	0	0.962
		±90	(−1.771)	±90	(−0.767)
	0.9	0	2.183	0	0.934
		±90	(−3.851)	±90	(−1.642)

Table 5. Maximum stress of ellipsoidal inclusions for uniaxial tension in the x-direction ($N \to \infty$, $a/b = 0.5$).

$a/b = 0.5$		Matrix			
E_I/E_M	b/d	ψ (deg.)	σ_n	ψ (deg.)	σ_θ
					$\theta = \frac{1}{2}\pi$
	0			0	2.480
	0.2			0	2.481
	0.5			±1	2.490
0	0.7			±3	2.509
	0.8			±45	2.534
	0.9			±73	2.644
			$\theta = 0$		$\theta = \frac{1}{2}\pi$
	0	0	0.225	0	2.164
	0.2	0	0.225	0	2.165
	0.5	0	0.225	±1	2.170
0.1	0.7	0	0.227	±3	2.183
	0.8	0	0.228	±43	2.199
	0.9	0	0.230	±73	2.273
			$\theta = 0$		$\theta = 0$
	0	0	1.549	0	0.588
	0.2	0	1.549	0	0.588
	0.5	0	1.547	0	0.588
10	0.7	0	1.542	0	0.586
	0.8	0	1.538	0	0.585
	0.9	0	1.531	0	0.584
			$\theta = 0$		$\theta = 0$
	0	0	1.652	0	0.708
	0.2	0	1.653	0	0.708
	0.5	0	1.651	0	0.708
10^5	0.7	0	1.646	0	0.706
	0.8	0	1.642	0	0.704
		±90	(−1.351)	±90	(−0.685)
	0.9	0	1.635	0	0.701
		±90	(−2.942)	±90	(−1.289)

Table 6. Maximum stress of ellipsoidal inclusions for uniaxial tension in the z-direction ($N \to \infty$, $a/b = 1.0$).

$a/b = 1.0$		Matrix			
E_1/E_M	b/d	ψ (deg.)	σ_n	ψ (deg.)	σ_t
	0			0	2.045
	0.2			0	2.031
	0.5			0	1.884
0	0.7			0	1.756
	0.8			0	1.703
	0.9			0	1.657
	0	±90	0.192	0	1.854
	0.2	±90	0.191	0	1.843
	0.5	±90	0.170	0	1.731
0.1	0.7	±75	0.130	0	1.627
	0.8	±65	0.116	0	1.582
	0.9	±59	0.103	0	1.543
	0	±90	1.768	±90	0.670
	0.2	±90	1.780	±90	0.674
	0.5	±90	2.028	±90	0.768
10	0.7	±90	2.824	±90	1.085
	0.8	±90	3.903	±90	1.517
	0.9	±90	6.68	±90	2.73
	0	±90	1.938	±90	0.831
	0.2	±90	1.955	±90	0.838
	0.5	±90	2.298	±90	0.985
10^5	0.7	±90	3.495	±90	1.498
	0.8	±90	5.36	±90	2.33
	0.9	±90	11.5	±90	5.14

3.4. Relation between the maximum stress and the number of inclusion N

Figures 13 illustrate $\sigma_{n\max}$ vs. $1/N^2$ relation when $a/b = 1.0$ and $b/d = 0.9, 0.7, 0.5, 0.2$. It appears as though $\sigma_{n\max}$ is linearly related to $1/N^2$ for large N. Therefore, the limiting values of $\sigma_{n\max}$ for $N \to \infty$ can be obtained by extrapolation. For example, even in the case of $b/d = 0.9$ in Figure 5, two extrapolated values obtained from $N = 8, 7$ and from $N = 7, 6$ coincide with each other to the fourth digit.

Tables 3, 4, 5 shows maximum stresses σ_n or σ_θ with their positions at the innermost inclusion when $N \to \infty$ for uniaxial tension in the x-direction. Tables 6, 7, 8 show maximum stresses σ_n, σ_t with their positions at the innermost inclusion when $N \to \infty$ for uniaxial tension in the z-direction.

Table 7. Maximum stress of ellipsoidal inclusions for uniaxial tension in the z-direction ($N \rightarrow \infty$, $a/b = 2.0$).

$a/b = 2.0$		Matrix			
E_1/E_M	b/d	ψ (deg.)	σ_n	ψ (deg.)	σ_t
	0			0	3.312
	0.2			0	3.184
	0.5			0	2.598
0	0.7			0	2.344
	0.8			0	2.248
	0.9			0	2.165
	0	±90	0.289	0	2.683
	0.2	±90	0.280	0	2.607
	0.5	±62	0.203	0	2.233
0.1	0.7	±49	0.166	0	2.052
	0.8	±45	0.151	0	1.983
	0.9	±40	0.138	0	1.922
	0	±90	1.328	±90	0.482
	0.2	±90	1.357	±90	0.492
	0.5	±90	1.866	±90	0.681
10	0.7	±90	2.989	±90	0.141
	0.8	±90	4.127	±90	1.620
	0.9	±90	6.299	±90	2.574
	0	±90	1.378	±90	0.591
	0.2	±90	1.416	±90	0.606
	0.5	±90	2.084	±90	0.894
10^5	0.7	±90	3.835	±90	1.647
	0.8	±90	6.17	±90	2.630
	0.9	±90	12.8	±90	5.446

4. Conclusions

In this study, a row of ellipsoidal inclusions in an infinite body under tension in the x- and z-directions are considered in terms of singular integral equations of the body force method. The asymmetric tension problem in the x-direction is solved on the superposition of two auxiliary loads, biaxial tension in the xy-plane, and plane state of pure shear in the xy-plane. In order to satisfy the boundary conditions, the unknown functions are approximated by a linear combination of fundamental density functions and ploynomials. The present method is found to yield rapidly converging numerical results and smooth stress distribution along the boundary. The maximum stresses and interface stresses are shown in tables and figures for

Table 8. Maximum stress of ellipsoidal inclusions for uniaxial tension in the z-direction ($N \to \infty$, $a/b = 0.5$).

$a/b = 0.5$		Matrix			
E_I/E_M	b/d	ψ (deg.)	σ_n	ψ (deg.)	σ_t
	0			0	1.440
	0.2			0	1.438
	0.5			0	1.411
0	0.7			0	1.372
	0.8			0	1.350
	0.9			0	1.328
	0	±90	0.139	0	1.380
	0.2	±90	0.139	0	1.378
	0.5	±90	0.135	0	1.357
0.1	0.7	±90	0.122	0	1.322
	0.8	±90	0.105	0	1.302
	0.9	±77	0.078	0	1.282
	0	±90	2.668	±90	1.026
	0.2	±90	2.674	±90	1.029
	0.5	±90	2.811	±90	1.081
10	0.7	±90	3.283	±90	1.262
	0.8	±90	4.020	±90	1.548
	0.9	±90	6.359	±90	2.479
	0	±90	3.279	±90	1.405
	0.2	±90	3.290	±90	1.410
	0.5	±90	3.519	±90	1.508
10^5	0.7	±90	4.336	±90	1.858
	0.8	±90	5.680	±90	2.435
	0.9	±90	11.43	±90	4.87

various shape, spacing, and elastic ratio of inclusions. Tuchida's results for spheroidal cavities coincide with the present results to the fourth digit in most cases.

When $E_I/E_M > 1$, the primary feature of the interaction is a large compressive stress σ_n for uniaxial tension in the x-direction and a large tensile stress σ_n for uniaxial tension in the z-direction. When $E_I/E_M < 1$, the most important part of the interaction is a large tensile stress σ_θ for uniaxial tension in the x-direction, and a large tensile stress σ_t for uniaxial tension in the z-direction. When b/d and E_I/E_M are fixed, the interaction effects are dominant when a/b is large as shown in Figures 5–10. A linear relationship is found between the maximum stress and $1/N^2$, where N is the number of inclusions. Using these relationship, the limiting

values for $N \to \infty$ are obtained. The maximum stress for $N \to \infty$ are tabulated for uniaxial tension in the x- and z-directions.

References

Atsumi, A. (1960). Stresses in a circular cylinder having an infinite row of spherical cavities under tension, Trans. ASME. *Journal of Applied Mechanics Series E* **27**(1), 87–92.

Donnel, L.H. (1941). Stress concentrations due to elliptical discontinuities in plates under edge forces. *Ann. Vol. T.* Von Karman, Calif. Inst. Tech. 293–309.

Edwards, R.H. (1952). Stress concentrations around spherical inclusions and cavities, Trans. ASME. *Journal of Applied Mechanics* **19**(1), 19–30.

Eshelby, J.D. (1975). The determination of the elastic field of an ellipsoidal inclusion, and related problems. *Proceedings of the Royal Society A* **241**, 376–396.

Eshelby, J.D. (1959). The elastic field outside an ellipsoidal inclusion. *Proceedings of the Royal Society A* **252**, 561–569.

Eubanks, R.A. (1956). Stress interference in three-dimensional torsion, Trans. ASME. *Journal of Applied Mechanics Series E* **32**(1), 21–25.

Goree, J.G. and Wilson, H.B. (1967). Axisymmetrc torsional stresses in a solid containing two partially bonded rigid spherical inclusions, Trans. ASME. *Journal of Applied Mechanics Series E* **34**(2), 313–320.

Isida, M. and Igawa, H. (1994). Some asymtotic behaviour and formulate of stress intensity factors for collinear and parallel cracks under various loadings. *International Journal of Fracture* **65**, 247–259.

Miyamoto, H. (1957). On the problem of the theory of elasticity for a region containing more than two spherical cavities (First report, theoretical calculatiolns). *Translation of the Japanese Society of Mechanical Engineering* (in Japanese) **23**(131), 431–436.

Nisitani, H. (1963). On the tension of an elastic body having an infinite row of spheroidal cavities. *Translation of the Japanese Society of Mechanical Engineering* (in Japanese) **29**(200), 765–768.

Nisitani, H. (1967). The two-dimensional stress problem solved using *sn* electric digital computer. *Journal of the Japanese Society of Mechanical Engineering* **70**, 627–632. [(1969), *Bulletin of Japanese Society of Mechanical Engineering* **11**, 14–23.]

Nisitani, H. (1968). Approximate calculation method of interaction between notches and its applications. *Journal of the Japanese Society of Mechanical Engineering* (in Japanese) **71**(589), 35–47.

Noda, N.A. and Matsuo, T. (1995). Singular integral equation method in the analysis of interaction between crack and defects, Fracture Mechanics: 25th Volume, *ASTM STP 1220*, (ed. Erdogan, F.), 591–605.

Noda, N.A. and Matsuo, T. (1997). Analysis of a row of elliptical inclusions in an plate using singular integral equations. *International Journal of Fracture* **83**, 315–336.

Noda, N.A. and Matsuo, T. (1998). Singular integral equation method in the analysis of interaction between elliptical inclusions. ASME *Journal of Applied Mechanics* **65**, 310–319.

Noda, N.A. and Tomari, K. (1998). Fundamental solution and its application for stress analysis of axisymmetric body under asymmetric uniaxial tension. *Bulletin of the Kyushu Institute of Technology* (in Japanese) **70**, 7–12.

Noda, N.A., Tomari, K. and Matsio, T. (1999). Interaction effect between ellipsoidal inclusions in an infinite body under asymmetric unixial tension. *JSME International Journal*, Series I, (submitted).

Noguchi, H., Nisitani, H., Goto, H. and Mori, K. (1987). Semi-infinite body with a semi-ellipsoidal pit under tension. *Translation of the Japanese Society of Mechanical Engineering* **53**(488), 820–826. [(1989). *JSME INternational Journal*, Series I **32**(1), 14–22].

Shelly, J.F. and Yu, Yi-Yuan (1966). The effect of two rigid spherical inclusions on the stresses in an infinite elastic solid. Trans. ASME, *Journal of the Applied Mechanics Series E* **33**(1), 68–74.

Shioya, S. (1970). Tension of a infinite thin plate having two equal circular inclusions. *Translation of the Japanese Society of Mechanical Engineering* (in Japanese) **36**, 886–897.

Tuchida, E., Nikahara, I. and Kodama, M. (1976). Asymmetric problem of elasitc body containing several spherical cavities (First Report: Two spherical cavities in an elastic body). *Translation of the Japanese Society of Mechanical Engineering* (in Japanese) **42**(353), 46–54.

Tuchida, E., Uchiyama, N., Nakahara, I. and Kodama, M. (1978), Asymmetric problem of elastic body containing several spherical cavities (Second report: three spherical cavities in an elastic body). *Translation of the Japanese Society of Mechanical Engineering* (in Japanese) **44**(382), 1876–1883.